

MRI reveals differential regulation of *retinal* and *choroidal* blood volumes in rat retina

Govind Nair^{a,b}, Yoji Tanaka^b, Moon Kim^e, Darin E. Olson^{c,e}, Peter M. Thulé^{c,e},
Machelle T. Pardue^{d,e}, Timothy Q. Duong^{f,g,h,i,*}

^a Graduate School of Biomedical Science, University of Massachusetts Medical School, Worcester, MA, USA

^b Yerkes Imaging Center, Emory University, Atlanta, GA, USA

^c Department of Medicine, Division of Endocrinology, Metabolism, and Lipids, Emory University, Atlanta, GA, USA

^d Department of Ophthalmology, Emory University, Atlanta, GA, USA

^e Atlanta Veterans Affairs Medical Center, Atlanta, GA, USA

^f Research Imaging Institute, Department of Ophthalmology, University of Texas Health Science, San Antonio, TX, USA

^g Research Imaging Institute, Departments of Radiology, University of Texas Health Science, San Antonio, TX, USA

^h Research Imaging Institute, Departments of Physiology, University of Texas Health Science, San Antonio, TX, USA

ⁱ South Texas Veterans Health Care System, San Antonio, TX, USA

ARTICLE INFO

Article history:

Received 25 June 2010

Revised 10 August 2010

Accepted 8 September 2010

Available online 17 September 2010

ABSTRACT

The retina is nourished by two unique (*retinal* and *choroidal*) circulations. The lack of depth-resolved blood volume (BV) imaging techniques hampers investigation of vascular-specific regulation of the retina *in vivo*. This study presents a high-resolution, laminar-specific magnetic resonance imaging (MRI) study to image *retinal* and *choroidal* BVs, their responses to physiologic challenges in normal and Royal-College-of-Surgeons (RCS) rats (a model of retinal degeneration). *Retinal* and *choroidal* BVs were imaged by MRI ($30 \times 30 \times 800 \mu\text{m}$) with intravascular administration of monocrystalline iron oxide nanocolloid (MION) contrast agent. Relative baseline BV and BV changes due to physiologic challenges were calculated in normal and RCS rat retinas. BV-MRI revealed two well-resolved *retinal* and *choroidal* vascular layers located on either side of the retina and an intervening avascular layer. The ratio of *choroidal:retinal* BV in normal rats at baseline was 9.8 ± 3.2 in control rat retinas ($N = 7$). Hyperoxia decreased *retinal* BV ($-51 \pm 17\%$, $p < 0.05$) more than *choroidal* BV ($-28 \pm 14\%$), and hypercapnia increased *retinal* BV ($52 \pm 11\%$, $p < 0.01$) more than *choroidal* BV ($12 \pm 11\%$). BV-MRI in degenerated retinas of RCS rats ($N = 7$) revealed thinning of the avascular layer and an increase in relative baseline *retinal* and *choroidal* BVs. Only hypercapnia-induced BV changes in the *retinal* vasculature of RCS rats were significantly different (smaller) from controls ($p < 0.05$). These findings suggest that BV in both retinal vasculatures is regulated. The relative baseline BV in both vasculatures increased in retinal degeneration. BV-MRI provides clinically relevant data that may prove useful for early detection and longitudinal probing of retinal diseases, and could complement optical imaging techniques.

© 2010 Elsevier Inc. All rights reserved.

Introduction

The retina is nourished by two distinct – *retinal* and *choroidal* – vasculatures. *Retinal* vessels – coursing on the surface of the retina, within the ganglion cell layer, inner plexiform layer and inner nuclear layer – are characterized by relatively low blood flow (BF) and a large arterio-venous pO_2 difference (similar to the brain). *Choroidal*

vessels – located external to the photoreceptor layer, and sandwiched between the retinal pigment epithelium and sclera – are characterized by relatively high BF and a low arterio-venous pO_2 difference. The outer nuclear layer and the photoreceptor segments are avascular (Harris et al., 1998). Importantly, sympathetic autonomous innervations play a significant role in *choroidal* BF regulation, while the *retinal* vasculature is autoregulated in a manner similar to cerebral vessels (Laties, 1967; Steinle et al., 2000). Microsphere measurements showed that basal *choroidal* BF is many times larger than *retinal* BF (Bill, 1984). Analysis by oxygen polarographic electrodes showed that tissue oxygenation profiles differ between the two vasculatures in response to physiologic challenges (Yu et al., 2000). These findings suggest divergent regulation of *retinal* and *choroidal* vessels. Moreover, *retinal* and *choroidal* regulation may respond differently to various retinal diseases, such as retinal ischemia, diabetic retinopathy, and retinitis pigmentosa.

Abbreviations: BF, blood flow; BV, blood volume; BOLD fMRI, blood-oxygenation-level-dependent functional MRI; MION, monocrystalline iron oxide nanocolloid; MRI, magnetic resonance imaging; RCS, Royal College of Surgeons; T_2^* , effective spin-spin relaxation time; ΔR_2^* , rate constant.

* Corresponding author. Research Imaging Institute, MRI Division, 8403 Floyd Curl Dr, San Antonio, TX 78229, USA. Fax: +1 210 567 8152.

E-mail address: duongt@uthscsa.edu (T.Q. Duong).

The lack of non-invasive, depth-resolved BF or blood volume (BV) imaging techniques has limited investigation of hemodynamic regulation in the two vasculatures *in vivo*. Fluorescein angiography, indocyanin-green angiography, and laser Doppler flowmetry (LDF) (Riva et al., 1994) are capable of providing information on BF velocity and relative BF in the retina. Intrinsic optical imaging can measure relative BV changes in the retina (Nelson et al., 2005). Optical coherence tomography can visualize blood velocity in large *retinal* and *choroidal* vessels (Drexler and Fujimoto, 2008). While these optical approaches have contributed remarkably to our understanding of retinal pathophysiology, they cannot unambiguously resolve *retinal* and *choroidal* BVs or BFs at the capillary/tissue level. Optical techniques are also often hampered by disease-induced opacity of the vitreous humor, cornea and lens.

In contrast, magnetic resonance imaging (MRI) provides *in vivo* structural, physiological (i.e., BF, BV and oxygenation) and functional information without depth limitation. Although the spatial resolution of MRI is low compared to optical methods, advances in MRI technologies have made possible high resolution MRI of the retina (see review by Duong and Muir, 2009; Duong et al., 2008). Anatomy (Cheng et al., 2006; Shen et al., 2006), BF (Li et al., 2008), oxygenation (Duong et al., 2002), and functional (Duong et al., 2002) MRI of the retina, which is ~270 μm thick including the *choroid* (Cheng et al., 2006), have been reported. A recent blood-oxygenation-level-dependent (BOLD) functional MRI (fMRI) study reveals differential responses of the two vasculatures when challenged with hyperoxia or hypercapnia (Cheng et al., 2006). During hyperoxic challenge, *choroidal* BOLD responses were larger than *retinal* responses. In contrast, during hypercapnic challenge, the BOLD *choroidal* responses were minimal, while *retinal* responses were large. However, because the BOLD signal is a convolution of competing changes in oxygen metabolism, including BV, and BF, among other measurement parameters, deciphering the root causes of altered BOLD signals remains difficult (Ogawa et al., 1993). Direct measurement of a single physiological parameter (such as BV and BF which are tightly coupled to each other under normal physiological conditions) may illuminate the phenomenon underlying differential vascular-specific responses in the retina.

The present study describes a high-resolution ($30 \times 30 \times 800 \mu\text{m}$) BV-MRI approach using a blood-pool MRI contrast agent – monocrySTALLINE iron oxide nanocolloid (MION) (Mandeville et al., 1998) which reduces blood water signals via enhanced magnetic susceptibility and thus allows highly sensitive measurement of the total relative BV at the tissue level without the need to visualize individual vessels. BV-MRI was applied to investigate layer-specific baseline BV and BV fMRI changes associated with hyperoxic and hypercapnic challenges in normal rat retina and in a retinal degeneration model – the Royal-College-of-Surgeons (RCS) rat (Dowling and Sidman, 1962) which has a genetic defect shared by many patients with autosomal-recessive retinitis pigmentosa (Gal et al., 2000).

Materials and methods

Animal preparations

Experiments were performed on normal adult male Long Evans rats (350–450 g, $N = 7$) and RCS rats (350–450 g, $N = 7$). Femoral vein was catheterized under 2% isoflurane for the administration of the intravascular BV contrast agent, MION (5 mg/kg), and a femoral artery was catheterized for blood pressure monitoring. The animal was placed in a MRI-compatible stereotaxic headset with a feedback-regulated warm-water circulating pad. A thin layer of methylcellulose was applied to the corneal surface to prevent desiccation. During MRI, the animal was maintained with ~1% isoflurane anesthesia, mechanically ventilated, and paralyzed with pancuronium bromide (1 mg/kg/h, ip). End-tidal CO_2 (Surgivet capnometer), heart rate and arterial oxygen saturation

(Nonin-8600), and rectal temperature (Digisense from Cole Palmer) were maintained within normal physiological ranges unless otherwise perturbed. This protocol yielded stable animal preparation for prolonged multiple measurements (Cheng et al., 2006; Li et al., 2008).

Inhalation stimuli

Hyperoxic (100% O_2) and hypercapnic (5% CO_2 , 21% O_2 , balance N_2) challenges were used to modulate the BV. Ambient air was used as baseline. Images were acquired continuously for 6 min during baseline and 6 min during hyperoxic or hypercapnic challenge. A break of 10–15 min was given between each stimulus. This break has been shown previously to be more than sufficient for the systemic circulation to return to baseline as demonstrated by MRI monitoring of BF and oxygenation (i.e., BOLD), exhaled O_2 and CO_2 monitoring as well as blood-gas measurements in previous rat brain studies (Sicard and Duong, 2005; Liu et al., 2004). Typically, two trials of both hyperoxia and hypercapnia were studied on the same animal and the presentation order of different physiologic challenges was at random, with the entire study lasting ~4 h including animal preparations. The relative baseline BV was calculated from the baseline measurement of hypercapnia and hyperoxia, before and after MION injection. The percentage change in BV during stimulus was calculated from images acquired during baseline and gas challenge, before and after MION administration.

MRI methods

MRI studies were performed on a Bruker 7-Tesla/30-cm magnet and a 40 G/cm B-GA12 gradient insert (Billerica, MA). A small circular surface coil (inner diameter ~7 mm) was placed on the left eye. Magnetic field homogeneity was optimized on an isotropic voxel encompassing the entire eye. A single sagittal imaging slice bisecting the center of the eye and the optic nerve head was used to minimize partial-volume effect. Serial BV-MRI was acquired before and after MION injection using T_2^* -weighted images with a gradient-echo sequence, 200 ms repetition time (TR), 6.5 ms echo time (TE), $7.7 \times 7.7 \text{ mm}$ field of view, 256×256 matrix giving an in-plane resolution of $30 \times 30 \mu\text{m}$, and 800 μm slice thickness.

Histology

Standard histology of the retina was analyzed on slices carefully chosen to match the MRI slices. Eyes were enucleated following anesthetic overdose and the sagittal plane marked on the eyeball using permanent marker. The eyes were immersion fixed overnight in 2% paraformaldehyde/2% glutaraldehyde and subsequently rinsed in 0.1 M phosphate buffer, dissected to isolate the posterior eyecup, divided into two halves along the sagittal plane, embedded in epoxy-resin, and sectioned at 5 μm for toluidine blue staining. Images of the sections at the level of the optic nerve, which approximately corresponded to the MRI slices, were captured under 20 \times magnification using an image analysis program (Image Pro, Cybernetics).

Data analysis

Image analysis employed codes written in Matlab (MathWorks Inc.) and STIMULATE software (University of Minnesota). Images were corrected for possible motion and drift (Cheng et al., 2006). BV index was calculated pixel-by-pixel from T_2^* -weighted MRI before and after MION injection, as the total concentration of MION in a pixel, and therefore the change in R_2^* after injection, was proportional to the blood volume in the pixel (Mandeville et al., 1998). Changes in transverse relaxation rate ($\Delta(1/T_2^*)$ or ΔR_2^*) acquisitions were calculated as $\Delta R_2^* = -\ln(S/S_0)/TE$, where S/S_0 is the signal relative to the value before MION injection, and TE the echo time.

The *magnitude BV change* associated with stimulation was calculated from images before and after stimulus as $\Delta BV = (\Delta R_2^*_{[post-MION]} - \Delta R_2^*_{[pre-MION]}) / \Delta R_2^*_{[pre-MION]}$, where the pre-MION signal change arises from the stimulus-evoked BOLD (deoxyhemoglobin) effect (Mandeville et al., 1998) and the post-MION signal change arises from both the stimulus-evoked MION and BOLD effects. Magnitude changes assumed that blood MION concentrations between animals were similar, which was achieved by using weight based dosage (5 mg/kg) in rats of similar size.

To minimize errors due to partial-volume, automated profile analysis (Cheng et al., 2006) of ΔR_2^* image (blood volume index) was performed, instead of region-of-interest analysis. The retina was first detected using an edge-detection technique. Radial projections perpendicular to the vitreous boundary were then obtained with (3 \times) spatial interpolation. Some interpolations were necessary for automation and such spatial interpolation does not significantly alter the magnitude or width of the signals being measured (Cheng et al., 2006). BV was determined as a function of distance from the optic nerve head. BV profiles were also plotted across the retinal thickness. The peak ΔR_2^* profile was taken as BV index, and the thickness of individual peaks at half-maximum height (full-width-at-half-maximum, FWHM) was determined to be the layer thickness. Blood volume percent changes (i.e., changes in ΔR_2^*) due to hyperoxia and hypercapnia relative to baseline (air) were tabulated. All reported values and error bars on graphs are mean \pm SD. A two-tailed student's t-test was performed for statistical comparison between groups. Paired t-test was used for comparison of *choroidal* to *retinal* BV and unpaired t-test was used for comparison between control and RCS groups. A $p < 0.05$ was taken to be statistically significant.

Results

Rat physiological parameters (body temperature, respiration rate, blood pressure, pO_2 , and pCO_2) were maintained within normal values over the course of the experiment, unless intentionally perturbed using hyperoxic or hypercapnic challenge. There were no significant changes to baseline physiologic parameters due to the injection of MION. The end-tidal CO_2 ($EtCO_2$) measured before the injection of MION (30 ± 2 mm Hg) was not different from that

measured after the injection (29.9 ± 1.9 mm Hg, $p > 0.9$). The mean arterial blood pressure before MION administration (MABP: 109 ± 20 mm Hg) was not statistically different from after the MION injection (115 ± 11 mm Hg, $p > 0.8$). Similarly, heart rate was not statistically different before and after the MION injection (397 ± 37 bpm before versus 406 ± 37 after, $p > 0.6$). The $EtCO_2$ decreased by $10 \pm 3\%$ ($p < 0.01$) during hyperoxia and increased by $148 \pm 2\%$ during hypercapnic challenges, as expected ($p < 0.01$). There were no significant changes in any other measured physiologic parameter measured during the systemic gas challenges. Rats were allowed to recover from inhalation for 10–15 min after each physiologic stimulus.

Basal BV in control and P90 RCS rats

Fig. 1 shows a T_2^* -weighted MRI before and after intravenous MION injection in a normal rat, and the calculated relative baseline BV image. T_2^* -weighted MRI signals on either side of the retina were attenuated after MION injection. The relative basal BV image, derived from changes in the spin–spin relaxation rate constant (ΔR_2^*) before and after MION injection, delineated the high BV signals on either side of the retina, corresponding to the *retinal* and *choroidal* vascular layers. The middle avascular layer in the retina, lens and vitreous or aqueous humor showed no significant BV signals. However, significant BV signals were detected in the iris, ciliary body and optic nerve head as expected because these structures have substantial blood flow. Some signal contrasts were observed on the corneal surface, likely due to subtraction errors in regions of high magnetic susceptibility artifacts.

Fig. 2 shows the relative baseline BV as a function of distance from the optic nerve head in a normal rat. *Choroidal* BV was relatively uniform along the length of the retina with no significant difference between the central and peripheral retina. In contrast, *retinal* BV was maximal around the optic nerve head. To avoid averaging over heterogeneous regions, group data were obtained from two regions of ~ 0.3 mm each at 1 mm superior and inferior to the optic nerve head (see Fig. 3a, inset).

In control rats the BV profile taken across the retinal thickness showed a *retinal* and *choroidal* layer thickness (FWHM) of 60 ± 24 and 83 ± 11 μ m (mean \pm SD, $N = 7$), respectively, (Fig. 3a), with a clear

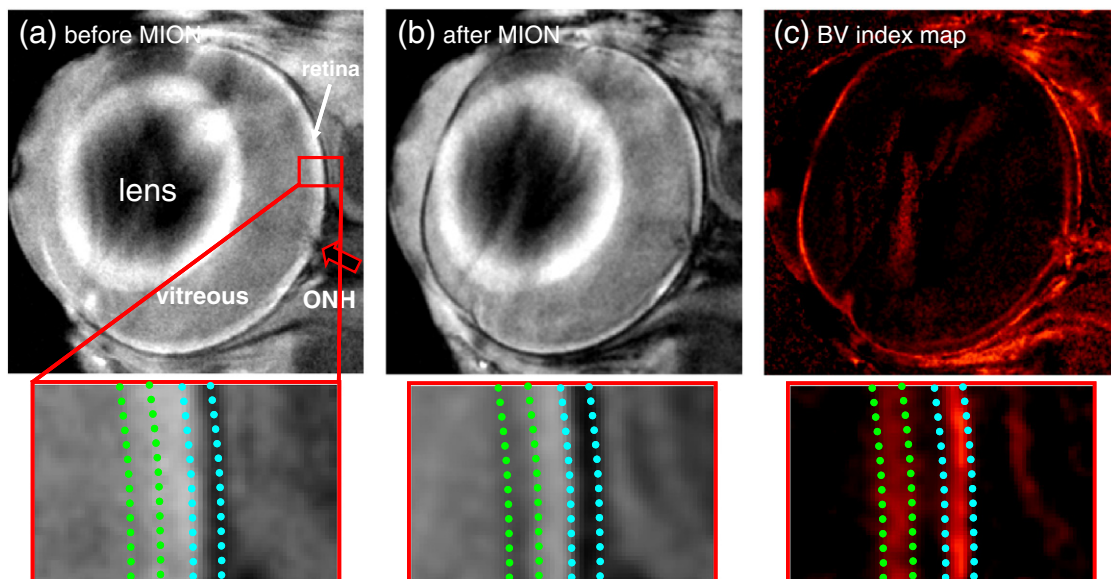


Fig. 1. T_2^* -weighted MRI at 30×30 μ m in-plane resolution of a rat eye (a) before and (b) after MION from a representative normal rat. (c) Relative baseline blood volume (ΔR_2^*) map clearly delineates the *retinal* and *choroidal* vascular layers and the avascular layer in between. Arrow indicates the location of the optic nerve head (ONH).

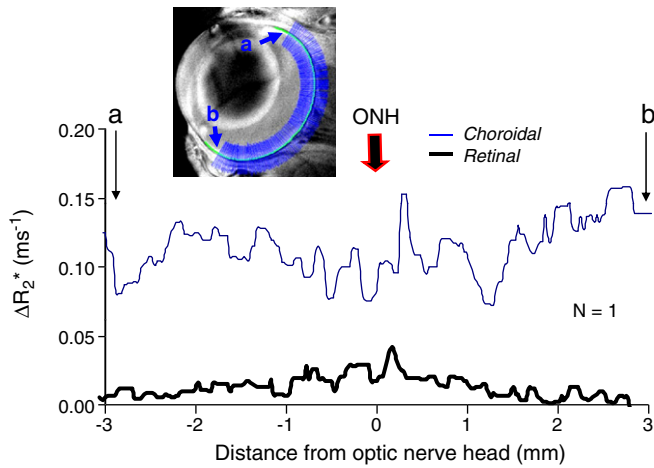


Fig. 2. Layer-specific baseline blood volume indices as a function of distance from the optic nerve head (ONH) from a representative control rat. *Choroidal* blood volume was substantially higher than *retinal* blood volume. The *retinal* profile peaks at the optic nerve head whereas the *choroidal* profile is relatively uniform. Data were obtained from superior to inferior retina (points a to b).

visualization of the avascular layer possible. The peak-to-peak separation was $203 \pm 25 \mu\text{m}$. By contrast, in P90 RCS rats MRI revealed marked thinning of the avascular photoreceptor layer, the two peaks being separated by $131 \pm 18 \mu\text{m}$ (in grey, $p < 0.01$). The *retinal* and *choroidal* layer thicknesses (as derived by extending the individual peaks in the profile plots) in the RCS rats by MION MRI were 50 ± 11 and $73 \pm 7 \mu\text{m}$ ($N = 7$), respectively, which were not statistically different from those of the age-matched controls.

The group-averaged relative basal BV (defined as the peak value of ΔR_2^* profile) of the *retinal* and *choroidal* vascular layers in normal and age-matched RCS rats is shown in Fig. 3b. The BV peak ratio of *choroidal* to *retinal* profile was 9.8 ± 3.2 in control rats, and 8.9 ± 2.8 in P90 RCS rats ($p > 0.5$). The area-under-the-curve ratio of the *choroidal* to *retinal* BV profile was 12.7 ± 4.3 in control rats and 13 ± 4 in P90 RCS rats, which was also not statistically different from controls. Importantly, baseline *retinal* and *choroidal* BVs were markedly higher in RCS (71% and 55%, respectively) compared to age-matched controls. Retinal degeneration in P90 RCS rats was confirmed by histology, in which only a thin debris layer was observed in place of the photoreceptors and photoreceptor segments and the total thickness was markedly reduced (Fig. 3c).

Stimulus-induced BV changes in control rats

Vascular layer-specific BV changes associated with hyperoxia and hypercapnia relative to air (baseline) were analyzed (Fig. 4). Both *choroidal* and *retinal* vessels exhibited hyperoxia-induced vasoconstriction and hypercapnia-induced vasodilation. Hyperoxia-induced BV percent change was larger in the *retinal* vasculature ($51 \pm 17\%$) compared to the *choroidal* vasculature ($28 \pm 14\%$) ($p < 0.01$). Similarly, hypercapnia-induced BV percent change was larger in the *retinal* vasculature ($52 \pm 11\%$) compared to the *choroidal* vasculature ($12 \pm 11\%$) ($p < 0.01$). There were no statistically significant stimulus-induced changes in the thickness of either the *retinal* or *choroidal* vascular layer ($p > 0.5$).

Stimulus-induced BV changes in RCS rats

BV fMRI associated with hyperoxia and hypercapnia was analyzed in RCS rat retinas in comparison with controls. Hyperoxia-induced BV changes in RCS rat retinas decreased by $51 \pm 12\%$ in the *retinal*

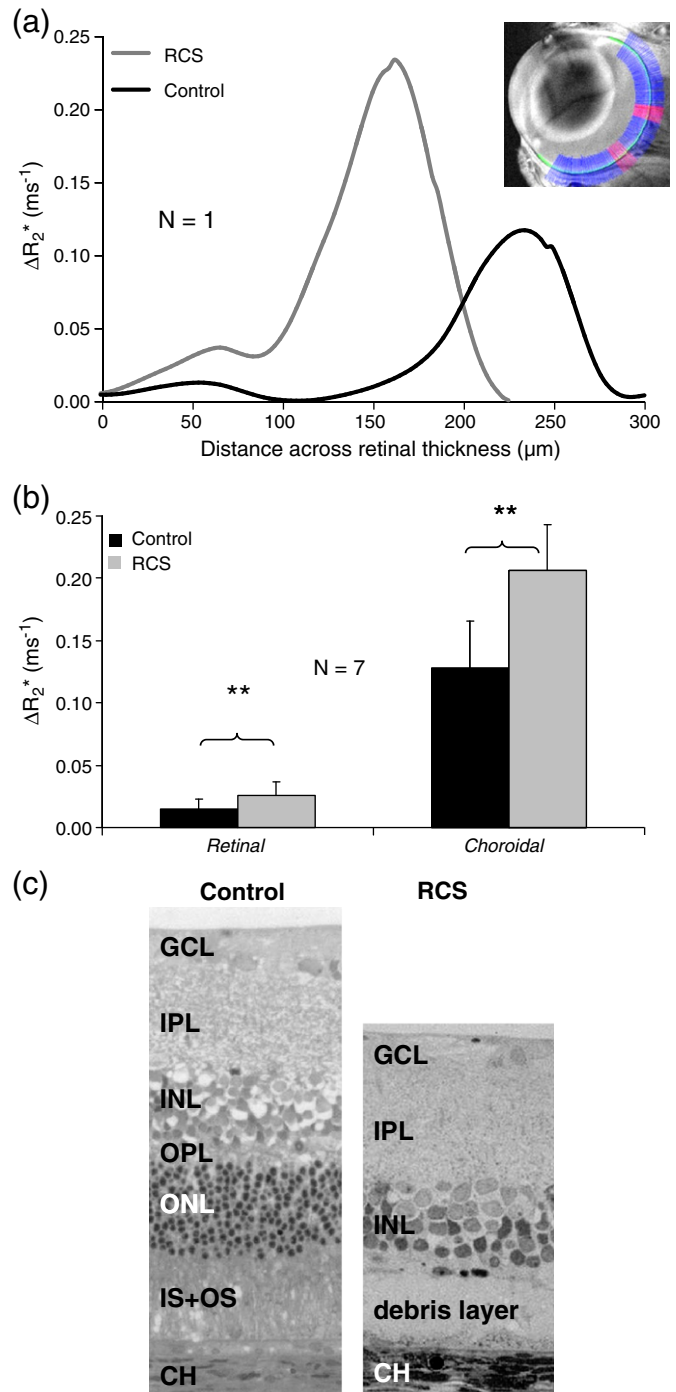


Fig. 3. (a) Profile plots of the baseline blood volume across the retinal thickness from a representative control and Royal-College-of-Surgeons (RCS) rats at P90. Inset: lines indicate radial projections across the retina. To avoid averaging spatial heterogeneity, BV indices were tabulated over 0.3 mm strip at $\pm 1 \text{ mm}$ away from the optic nerve head (red lines). (b) Group-averaged relative baseline blood volume values were taken at the peak of the ΔR_2^* profiles. RCS retinas were thinner than normal age-matched controls as seen by the proximity of the blood volume peaks from *retinal* and *choroidal* vasculatures compared to age-matched controls. The relative baseline blood volume was higher in both *retinal* and *choroidal* vascular layers in the RCS rats. (c) Toluidine-stained histological sections show the thinning of an RCS rat retina compared to an age-matched control. (GCL: ganglion cell layer; IPL: inner plexiform layer; INL: inner nuclear layer; OPL: outer plexiform layer; ONL: outer nuclear layer; IS + OS: inner and outer segments of the photoreceptors; CH: *choroidal* vasculature). * $p < 0.05$, ** $p < 0.01$.

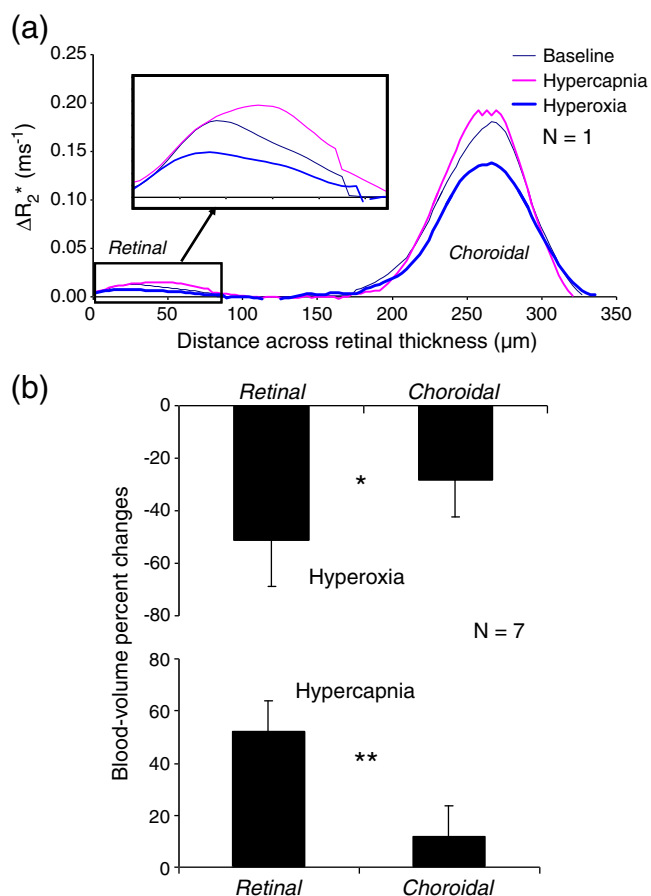


Fig. 4. Layer-specific blood volume changes responding to hyperoxia and hypercapnia from (a) a representative control rat. (b) Group-averaged retinal and choroidal blood volume changes due to hyperoxia and hypercapnia (* $p < 0.05$, ** $p < 0.01$).

vasculature and $22 \pm 11\%$ in the *choroidal* vasculature compared to baseline ($p < 0.01$), neither of these changes were significantly different from age-matched controls ($p > 0.05$). Hypercapnia-induced BV changes increased by $32 \pm 18\%$ in the *retinal* vasculature, and $9 \pm 10\%$ in the *choroidal* vasculature during hypercapnic stimulus ($p < 0.01$ versus baseline) in RCS rats. Only the hypercapnia-induced BV changes in the *retinal* vasculature of RCS rats were significantly different (smaller) from age-matched controls ($p < 0.05$).

Discussion

Blood volume MRI revealed two distinct laminar signals that correspond to the *retinal* and *choroidal* vascular layers bounding the retina, separated by the avascular layer in between. *Choroidal* BV was about ten times higher than *retinal* BV, as expected. fMRI based on BV changes detects vascular layer-specific responses to physiologic challenges and reveals that the *choroidal* blood vessels were less responsive to physiologic challenge than *retinal* vessels, indicative of differential hemodynamic regulation of the two vasculatures. In an accepted animal model of photoreceptor degeneration, MRI confirmed the disappearance of the outer nuclear layer and photoreceptor segments, as seen previously (Cheng et al., 2006). The baseline BV values in the *retinal* and *choroidal* vasculatures were elevated compared to age-matched controls. Only the hypercapnia-induced BV percent changes in the *retinal* vascular layer of the RCS rats were significantly different from controls. *Choroidal* and *retinal* vascular layer thickness and *choroidal:retinal* BV ratio were unaltered by retinal degeneration. To our knowledge this is the first *in vivo* report of

vascular layer-specific BV-MRI and BV fMRI of vascular coupling to physiologic challenges in normal retinas and in a clinically relevant model of retinal disease.

Basal BV in normal animals

Non-invasive measurements of *retinal* and *choroidal* blood volumes *in vivo* have not been reported to our knowledge. Consistent with the vascular layout of the retina, BV-MRI signal of the *retinal* vasculature was highest close to the optic nerve head and declined toward the peripheral retina. All *retinal* vessels originate from the optic nerve head and surface *retinal* vascular density progressively decreases toward the periphery. In contrast, *choroidal* BV was relatively uniform across the entire retinal length. *Choroidal* vessels originate from multiple medial and lateral posterior ciliary arteries entering the *choroidal* at various locations (Hayreh, 1974). Consequently, the BV findings and the thicknesses of the *retinal* and *choroidal* vascular layers were consistent with known retinal anatomy.

While quantitative blood volume in the vasculature was not determined herein, the *choroidal* BV was determined to be ten times higher than *retinal* BV. This result is in good agreement with the higher blood flow observed in the *choroidal* than the *retinal* vasculature using microspheres as tracers in rhesus monkey retina (Bill, 1984) and a MRI measurement using arterial spin labeling technique capable of resolving quantitative retinal and choroidal blood flow (Muir and Duong, 2010 in press). This finding is also in agreement with an MRI study utilizing an intravascular contrast agent (Gd-DTPA, gadolinium diethylenetriamine penta-acetic acid) in which the subtraction of post and pre contrast images showed the *choroidal* vascular layer to be significantly more enhanced than the *retinal* vascular layer, albeit no quantitative analysis was performed (Cheng et al., 2006). The functional necessity of a high *choroidal* BV remains unclear. High BF and BV may be required to dissipate heat produced by incident light (Parver, 1980) and/or to maintain a large oxygen gradient to facilitate oxygen delivery to the avascular outer nuclear layer (Linsenmeier and Padnick-Silver, 2000) where the oxygen tension is close to zero under normal physiologic conditions. However, these hypotheses remain to be validated.

Stimulus-evoked BV changes in normal retinas

Only a few BF studies have utilized physiological challenges to characterize the retinal vasculatures. Hyperoxia has consistently been reported to decrease BF in the retina by 30% using the Heidelberg Retina Flowmeter (Sternn et al., 1997), and 60% using LDF (Eperson et al., 1975; Riva et al., 1983; Trokel, 1965). However, these techniques do not provide vascular layer specificity and are mostly sensitive to surface *retinal* vessels with unknown contributions from the *choroid*. Hyperoxia has also been reported to have little effect on *choroidal* BF when measured using LDF in the human macula where *retinal* vessels are largely absent (Riva et al., 1994). *Retinal* blood flow increases more significantly than *choroidal* blood flow post exercise in humans (Okuno et al., 2006).

The literatures on hypercapnic responses, on the other hand, are inconsistent. Inhalation of 10% CO_2 in air showed no significant vasodilation in the *retinal* vessels (Frayser and Hickam, 1964). Inhalation of carbogen (95% O_2 + 5% CO_2) increased the *choroidal* BF by $12.5 \pm 11.7\%$ but inter-subject variations were large (Geiser et al., 2000). At higher CO_2 concentrations, however, *retinal* BF was observed to increase 240% and *choroidal* BF was observed to increase 150% (arterial $\text{pCO}_2 = 80.9$ mm Hg, which we estimate to be $>15\%$ CO_2 , effectively) (Alm and Bill, 1972).

Oxygen electrode measurements (Yu et al., 2000) suggest differential tissue pO_2 responses in the two vasculatures when challenged with hyperoxia and carbogen (5% CO_2 , 95% O_2). Hyperoxia markedly enhanced pO_2 in the *choroid* but only mildly enhanced pO_2

in the *retinal* region. Tissue oxygenation under carbogen inhalation compared to oxygen inhalation was slightly higher in the *choroidal* region, but markedly higher in the *retinal* region.

A recent BOLD fMRI study (Cheng et al., 2006) also suggested differential oxygen responses to hyperoxia and hypercapnia in the two vascular layers. Hyperoxia induced a larger BOLD response in the outer *choroidal* band ($12 \pm 2\%$, $N = 8$) than the inner *retinal* band ($7 \pm 2\%$, $p < 0.01$). In contrast, hypercapnia induced a smaller BOLD response in the outer *choroidal* band ($1.6 \pm 1\%$, $N = 8$) than in the inner *retinal* band ($10 \pm 2\%$, $p < 0.01$). The BOLD signal is a convolution of competing changes in oxygen metabolism, BV, and BF. The current study provides direct evidence that BV in the two vasculatures is indeed differentially regulated, and BV-MRI provides a novel perspective on ocular hemodynamics. Based on the current data, we conclude that *choroidal* vessels vasoconstrict in response to hyperoxia and vasodilate in response to hypercapnia less than *retinal* vessels, but do autoregulate to a degree. Our findings support the notion that the *retinal* vessels are strongly autoregulated.

It is unknown how BV and BF are coupled in the retina. It is possible that BF–BV coupling in the retina is similar to that in the brain, and can be described via Grubb's relation ($\Delta BF = \Delta BV^{0.38}$) (Grubb et al., 1974). However, the BF–BV coupling in the retina may differ from that in the brain because of the unique characteristics of the *retinal* and *choroidal* vasculatures as discussed earlier (Laties, 1967; Steinle et al., 2000). BF measurements are needed.

BV and BV responses in RCS rat retinas

Photoreceptor degeneration in RCS rats is well characterized with prominent degeneration of the avascular layer as confirmed by BV peak separation, providing a good model to corroborate layer-specific BV findings. In addition, peak- ΔR_2^* in RCS *retinal* and *choroidal* vessels were 46% to 80% higher than age-matched wild-type rats in this study. Neovascularization has been reported in *retinal* vasculature of P120 RCS rats resulting in an almost 50% increase in superficial *retinal* capillary density (Seaton and Turner, 1992). Fluorescein and indocyanin-green angiography studies in ~P70 RCS rats reveal hyper-fluorescent regions, suggesting regions of neovascularization and formation of coiled vascular tufts (Seaton and Turner, 1992). Consistent with these observations, our studies indicate that the *choroidal* BV is 46%–61% higher and *retinal* BV is 51%–80% higher in the RCS retina than the normal retina.

It should be noted that the steady-state BV calculation by MRI assumes that there is no leakage of MION from either the *retinal* or *choroidal* vasculature in RCS rats, which could potentially result in an overestimation of the BV. The blood-retinal barrier in normal *retinal* vessels and the *retinal* pigment epithelium form the tight junctions to prevent leakage of large molecules such as indocyanin-green and MRI contrast agents. However, *retinal* vascular permeability has been shown to increase with age in RCS retina using fluorescein angiography (Satoh and Yamaguchi, 2000). A previous MRI study on RCS rats using Gd-DTPA as a vascular contrast agent revealed an apparent thickening of the *choroid*, suggesting that this layer is permeable to Gd-DTPA in *retinal* degeneration.

Our current finding of BV increase in RCS rats appears to be inconsistent with a previous study which reported a blood flow decrease in RCS rats using arterial spin-labeling technique without a use of contrast agent (Li et al., 2009). A possible explanation could be due to methodological differences, namely, that blood volume and blood flow parameters are different aspects of the physiology. Another possible explanation is that MION leakage overestimated BV. However, lack of ΔR_2^* changes due to MION in the vitreous, as well as lack of any time dependent ΔR_2^* in the *choroids* in either the control or RCS rats suggests that MION does not leak out of the *retinal* vasculature, up to 2 h following MION injection. Nonetheless, the implication is that BV-MRI, which measures tissue BV without the

need to visualize individual vessels, can be utilized to image BV abnormalities *in vivo*.

BV fMRI responses to hyperoxia in both *retinal* and *choroidal* vessels in RCS rat retinas are similar to normal controls, in reasonable agreement with a BOLD fMRI study which showed that hyperoxic responses in RCS rats were only slightly attenuated compared to controls (Cheng et al., 2006). Hypercapnia-induced BV changes in the *retinal* vasculature of RCS rats were significantly different (smaller) from controls ($p < 0.05$), consistent with BOLD fMRI findings (Cheng et al., 2006). Hypercapnia-induced BV changes in the *choroidal* vessels in RCS rats were not statistically different from controls ($p > 0.05$). In contrast, a previous report found that hypercapnia-induced BOLD changes in *choroidal* vasculature of RCS rats were significantly different from controls although the hypercapnia-induced BOLD changes in normal *choroid* are already small (Cheng et al., 2006). Further studies are needed to address these discrepancies. We found no other publication using other imaging techniques to study hemodynamics and vascular responses of *retinal* degeneration. These findings underscore the utility of BV fMRI to image changes in BV and vascular reactivity associated with *retinal* diseases.

In summary, we demonstrate a novel MRI application to image layer-specific BV in the retina, providing important insights into the unique *retinal* and *choroidal* hemodynamic regulation in normal and diseased retinas *in vivo*. This approach may prove useful to monitor BV, its vascular reactivity, permeability and neovascularization associated with diseases in the two vasculatures of the retina.

Acknowledgments

The following funding sources are acknowledged: NIH/NEI (R01EY014211, R01EY018855) to TQD, VA Career Development (TQD and DEO), VA MERIT (TQD, PMT and MTP), Research to Prevent Blindness (MTP).

References

- Alm, A., Bill, A., 1972. The oxygen supply to the retina. II. Effects of high intraocular pressure and of increased arterial carbon dioxide tension on uveal and *retinal* blood flow in cats. *Acta Physiol. Scand.* 84, 306–319.
- Bill, A., 1984. Circulation in the eye. In: Renkin, E.M., Michel, C.C. (Eds.), *Handbook of Physiology Part 2 in Microcirculation*. American Physiological Society, Bethesda, MD, pp. 1001–1035.
- Cheng, H., Nair, G., Walker, T.A., Kim, M.K., Pardue, M.T., Thule, P.M., Olson, D.E., Duong, T.Q., 2006. Structural and functional MRI reveals multiple *retinal* layers. *Proc. Natl. Acad. Sci. USA* 103, 17525–17530.
- Dowling, J.E., Sidman, R.L., 1962. Inherited *retinal* dystrophy in the rat. *J. Cell Biol.* 14, 73–109.
- Drexler, W., Fujimoto, J.G., 2008. State-of-the-art *retinal* optical coherence tomography. *Prog. Retin. Eye Res.* 27, 45–88.
- Duong, T.Q., Muir, E.R., 2009. Magnetic resonance imaging of the *Retina*. *Jpn. J. Ophthalmol.* 53, 352–367.
- Duong, T.Q., Ngan, S.-C., Ugurbil, K., Kim, S.-G., 2002. Functional magnetic resonance imaging of the *retina*. *Invest. Ophthalmol. Vis. Sci.* 43, 1176–1181.
- Duong, T.Q., Pardue, M.T., Thule, P.M., Olson, D.E., Cheng, H., Nair, G., Li, Y., Kim, M., Zhang, X., Shen, Q., 2008. Layer-specific anatomical, physiological and functional MRI of the *retina*. *NMR Biomed* 21, 978–996.
- Eperson, G., Johnson, M., David, N.J., 1975. The effect of arterial pO_2 on relative *retinal* blood flow in monkeys. *Invest. Ophthalmol. Vis. Sci.* 14, 342–352.
- Frayser, R., Hickam, J.B., 1964. *Retinal* vascular response to breathing increased carbon dioxide and oxygen concentrations. *Invest. Ophthalmol. Vis. Sci.* 3, 427–431.
- Gal, A., Li, Y., Thompson, D.A., Weir, J., Orth, U., Jacobson, S.G., Apfelstedt-Sylla, E., Vollrath, D., 2000. Mutations in MERTK, the human orthologue of the RCS rat *retinal* dystrophy gene, cause *retinitis pigmentosa*. *Nat. Genet.* 26, 270–271.
- Geiser, M.H., Riva, C.E., GDorner, G.T., Diermann, U., Luksch, A., Schmetterer, L., 2000. Response of *choroidal* blood flow in the foveal region to peroxia and hyperoxia-hypercapnia. *Curr. Eye Res.* 21, 669–676.
- Grubb Jr., R.L., Raichle, M.E., Eichling, J.O., Ter-Pogossian, M.M., 1974. The effects of changes in $PaCO_2$ on cerebral blood volume, blood flow, and vascular mean transit time. *Stroke* 5, 630–639.
- Harris, A., Kagemann, L., Cioffi, G.A., 1998. Assessment of human ocular hemodynamics. *Surv. Ophthalmol.* 42, 509–533.
- Hayreh, S.S., 1974. Submacular *choroidal* vascular pattern. Experimental fluorescein fundus angiographic studies. *Albrecht Von Graefes Arch. Klin. Exp. Ophthalmol.* 192, 181–196.

- Laties, A., 1967. Central retinal artery innervation. Absence of adrenergic innervation to the intraocular branches. *Arch. Ophthalmol.* 77, 405–409.
- Li, Y., Cheng, H., Duong, T.Q., 2008. Blood-flow magnetic resonance imaging of the retina. *Neuroimage* 39, 1744–1751.
- Li, Y., Cheng, H., Shen, Q., Kim, M., Thule, P.M., Olson, D.E., Pardue, M.T., Duong, T.Q., 2009. Blood-flow magnetic resonance imaging of retinal degeneration. *Invest. Ophthalmol. Vis. Sci.* 50, 1824–1830.
- Linsenmeier, R.A., Padnick-Silver, L., 2000. Metabolic dependence of photoreceptors on the choroid in the normal and detached retina. *Invest. Ophthalmol. Vis. Sci.* 41, 3117–3123.
- Liu, Z.M., Schmidt, K.F., Sicard, K.M., Duong, T.Q., 2004. Imaging oxygen consumption in forepaw somatosensory stimulation in rats under isoflurane anesthesia. *Magn. Reson. Med.* 52, 277–285.
- Mandeville, J.B., Marota, J.J., Kosofsky, B.E., Keltner, J.R., Weissleder, R., Rosen, B.R., 1998. Dynamic functional imaging of relative cerebral blood volume during rat forepaw stimulation. *Magn. Reson. Med.* 39, 615–624.
- Nelson, D.A., Krupsky, S., Pollack, A., Aloni, E., Belkin, M., Vanzetta, I., Rosner, M., Grinvald, A., 2005. Special report: noninvasive multi-parameter functional optical imaging of the eye. *Ophthalmic Surg. Lasers Imaging* 36, 57–66.
- Ogawa, S., Menon, R.S., Tank, D.W., Kim, S.-G., Merkle, H., Ellermann, J.M., Ugurbil, K., 1993. Functional brain mapping by blood oxygenation level-dependent contrast magnetic resonance imaging. *Biophys. J.* 64, 800–812.
- Okuno, T., Sugiyama, T., Kohyama, M., Kojima, S., Oku, H., Ikeda, T., 2006. Ocular blood flow changes after dynamic exercise in humans. *Eye* 20, 796–800.
- Parver, L.M., 1980. Choroidal blood flow as a heat dissipating mechanism in the macula. *Am. J. Ophthalmol.* 89, 641–646.
- Riva, C.E., Grunwald, J.E., Sinclair, S.H., 1983. Laser Doppler velocimetry study of the effect of pure oxygen breathing on retinal blood flow. *Invest. Ophthalmol. Vis. Sci.* 24, 47–51.
- Riva, C.E., Cranston, S.D., Grunwald, J.E., Petrig, B.L., 1994. Choroidal blood flow in the foveal region of the human ocular fundus. *Invest. Ophthalmol. Vis. Sci.* 35, 4273–4281.
- Satoh, T., Yamaguchi, K., 2000. Ocular fundus abnormalities detected by fluorescein and indocyanine green angiography in the Royal College of Surgeons dystrophic rat. *Exp. Anim.* 49, 275–280.
- Seaton, A.D., Turner, J.E., 1992. RPE transplants stabilize retinal vasculature and prevent neovascularization in the RCS rat. *Invest. Ophthalmol. Vis. Sci.* 33, 83–91.
- Shen, Q., Cheng, H., Pardue, M.T., Chang, T.F., Nair, G., Vo, V.T., Shonat, R.D., Duong, T.Q., 2006. Magnetic resonance imaging of tissue and vascular layers in the cat retina. *J. Magn. Reson. Imaging* 23, 465–472.
- Sicard, M., Duong, T.Q., 2005. Effects of hypoxia, hyperoxia and hypercapnia on baseline and stimulus-evoked BOLD, CBF and CMRO2 in spontaneously breathing animals. *Neuroimage* 25, 850–858.
- Steinle, J.J., Krizsan-Agbas, D., Smith, P.G., 2000. Regional regulation of choroidal blood flow by autonomic innervation in the rat. *Am. J. Physiol. Regul. Integr. Comp. Physiol.* 279, R202–R209.
- Sternn, K., Manapace, R., Rainer, G., Findl, O., Wolzt, M., Schmetterer, L., 1997. Reproducibility and sensitivity of scanning laser Doppler flowmetry using graded changes in PO2. *Br. J. Ophthalmol.* 81, 360–364.
- Trokel, S., 1965. Effect of respiratory gases upon choroidal hemodynamics. *Arch. Ophthalmol.* 73, 838–842.
- Yu, D.-Y., Cringle, S.J., Su, E.-N., Yu, P.K., 2000. Intraretinal oxygen levels before and after photoreceptor loss in the RCS rat. *Invest. Ophthalmol. Vis. Sci.* 41, 3999–4006.